Correlations between Crystallite/Particle Size and Photoluminescence Properties of Submicrometer Phosphors

Wei-Ning Wang,† W. Widiyastuti,† Takashi Ogi,† I. Wuled Lenggoro,‡ and Kikuo Okuyama*,†

Department of Chemical Engineering, Graduate School of Engineering, Hiroshima University, Higashi Hiroshima, 739-8527, Japan, and Institute of Symbiotic Science and Technology, Tokyo University of Agriculture and Technology, Tokyo, 184-8588, Japan

Received December 6, 2006. Revised Manuscript Received January 26, 2007

Correlations between crystallite/particle size and the luminescent characteristics of submicrometer phosphors were investigated. Spray pyrolyzed europium doped yttrium oxide (Y_2O_3:Eu^{3+}) particles were selected as a model material. Crystallite size and the particle size were controlled independently. The morphology and crystallite structure were characterized by field-emission scanning electron microscopy, high-resolution transmission electron microscopy, X-ray diffraction, and selected area electron diffraction. Photoluminescence (PL) properties were examined by spectrofluorophotometry and an absolute PL quantum efficiency (QE) measurement system. Chemical analyses and elemental mapping were conducted by Fourier transform infrared spectrophotometry and STEM equipped with energy dispersive spectroscopy, respectively. The results revealed that the PL properties were strongly dependent on crystallite size, particle size, surface chemistry, and the distribution of europium inside the phosphor particles. The PL intensities and QE increased with increasing crystallite size and particle size. The effect of crystallite size on PL properties played a more important role than that of particle size.

1. Introduction

Inorganic luminescent materials (also known as phosphors), have been extensively studied for use as display materials and are currently in widespread use in applications of high definition television (HDTV), plasma display panels (PDP), cathode ray tube (CRT), and field emission displays (FED).[1,2] Among these luminescent materials, rare earth doped phosphors, for example, red luminescent phosphors doped with trivalent europium (Eu^{3+}) ions, because of intra-configuration $f-f$ transitions, are of technological importance because they are widely used in color displays and fluorescent lamps.[1] Microcrystalline yttrium oxide doped with Eu^{3+} (Y_2O_3:Eu^{3+}) represents a typical example and is considered to be one of the best red phosphors currently available.[3] In this work, Y_2O_3:Eu^{3+} was selected as a model material due to its many merits, such as good luminescent properties, stability in a vacuum, high melting point (∼ 2400 °C), and very high thermal conductivity.[4]

In the engineering of phosphors, there are three principal areas which must be studied and controlled so that the desired objectives of developing improved powder phosphors can be achieved, that is, (a) particle morphology and size (d_p); (b) stoichiometry and composition; and (c) surface chemistry.[5] To extend phosphors to high resolution applications, fine phosphor particles with a spherical morphology, homogeneous composition, and good surface properties would be highly desirable.[6]

A variety of methods have been applied to the preparation of phosphors for these purposes, including hydrothermal,[4] sol−gel,[7] copolymer micro-gel method,[8] precipitation,[9,10] bicontinuous cubic phase process,[11] combustion,[12] and spray pyrolysis methods.[13−16] Among these methods, the spray

* Corresponding author: e-mail okuyama@hiroshima-u.ac.jp; tel. +81-82-424-7716; fax +81-82-424-5494.
† Hiroshima University.
‡ Tokyo University of Agriculture and Technology.

(1) Blasse, G.; Grabmaier, B. C. *Luminescent Materials*; Springer-Verlag: Berlin, Germany, 1994.
(2) Feldmann, C.; Justel, T.; Ronda, C. R.; Schmidt, P. J. *Adv. Funct. Mater.* **2003**, *13*, 511.
(3) Vetrone, F.; Boyer, J.-C.; Capobianco, J. A. Luminescence, Optical Spectroscopy, and Applications of Rare Earth Doped Y_2O_3 Nanocrystals. In *Handbook of Luminescence, Display Materials, and Devices*; Nalwa, H. S., Rohwer, L. S., Eds.; American Scientific Publishers: Stevenson Ranch, CA, 2003; Vol. 2: Inorganic Display Materials, pp 141−186.
(4) Wan, J. X.; Wang, Z. H.; Chen, X. Y.; Mu, L.; Qian, Y. T. *J. Cryst. Growth* **2005**, *284*, 538.
(5) Vecht, A.; Gibbons, C.; Davies, D.; Jing, X. P.; Marsh, P.; Ireland, T.; Silver, J.; Newport, A.; Barber, D. *J. Vac. Sci. Technol. B* **1999**, *17*, 750.
(6) Wakefield, G.; Holland, E.; Dobson, P. J.; Hutchison, J. L. *Adv. Mater.* **2001**, *13*, 1557.
(7) Zhang, J. Y.; Zhang, Z. T.; Tang, Z. L.; Lin, Y. H.; Zheng, Z. S. *J. Mater. Process. Technol.* **2002**, *121*, 265.
(8) Martinez-Rubio, M. I.; Ireland, T. G.; Fern, G. R.; Silver, J.; Snowden, M. J. *Langmuir* **2001**, *17*, 7145.
(9) Jing, X.; Ireland, T.; Gibbons, C.; Barber, D. J.; Silver, J.; Vecht, A.; Fern, G.; Trowga, P.; Morton, D. C. *J. Electrochem. Soc.* **1999**, *146*, 4654.
(10) Silver, J.; Martinez-Rubio, M. I.; Ireland, T. G.; Fern, G. R.; Withnall, R. *J. Phys. Chem. B* **2001**, *105*, 948.
(11) Chien, W. C. *J. Cryst. Growth* **2006**, *290*, 554.
(12) Kottaisamy, M.; Jeyakumar, D.; Jagannathan, R.; Rao, M. M. *Mater. Res. Bull.* **1996**, *31*, 1013.
(13) Kang, Y. C.; Park, S. B.; Lenggoro, I. W.; Okuyama, K. *J. Mater. Res.* **1999**, *14*, 2611.
(14) Kang, Y. C.; Roh, H. S.; Bin Park, S. *Adv. Mater.* **2000**, *12*, 451.
(15) Hong, G. Y.; Yoo, K.; Moon, S. J.; Yoo, J. S. *J. Electrochem. Soc.* **2003**, *150*, H67.

10.1021/cm062887p CCC: $37.00
Published on Web 03/07/2007

pyrolysis method is potentially promising, since it is a simple, rapid, and continuous process, low cost, and can be used in the fabrication of diverse materials, including phosphors, with controllable sizes and compositions.[17] Particles prepared using the conventional spray pyrolysis (CSP) method are highly uniform in size and composition, with a spherical morphology, and have non-agglomeration characteristics, because of the microscale reactions that proceed inside a droplet. Submicrometer to micrometer sized particles are typically produced via the CSP method based on the one droplet to one particle assumption (ODOP).[18]

It is well-known that the majority of commercial phosphors in use today are in the micrometer size range (i.e., from one micrometer to a few ten micrometers). The optimization of luminescence intensity of Y_2O_3:Eu^{3+} particles by varying different parameters such as precursor concentration,[14] surface area and crystallite size (d_c),[19] morphologies,[20] synthesis technique and reactants,[7,8,11,21] Eu^{3+} concentration,[5] and so forth have been reported. Shea et al.[21] synthesized red-emitting $Y_3Al_5O_{12}$:Cr^{3+} and Y_2O_3:Eu^{3+} phosphors in the micrometer size range by means of an optimized combustion process. An increase in phosphor brightness with increasing reaction temperature, that is, crystallinity, was observed. The low-voltage (200−1000 V) cathodeluminescence (CL) efficiency of Y_2O_3:Eu^{3+} was also found to increase with increasing crystallite size, independent of the particle size, yet the particle morphology was irregular.[22] Joffin et al.[23] reported on the influence of microstructure and macrostructure on the luminescent properties of micrometer sized Y_2O_3:Eu^{3+} powders prepared by a spray pyrolysis method. Nevertheless, the as-prepared particles became hollow and broken after postannealing which may not be representative and would be inappropriate for industrial applications. The effects of surface area and crystallite size on the luminescent intensity of a Y_2O_3:Eu^{3+} phosphor prepared by spray pyrolysis were reported by Jung et al.[19] They found that Y_2O_3:Eu^{3+} particles with a smaller surface area showed a higher photoluminescence (PL) intensity. The PL intensities were also found to be linearly dependent on crystallite size. The same tendency was found for the influence of crystallite size on the PL intensity for other phosphors as well, such as Gd_2O_3:Eu^{3+}.[18] The morphology dependent luminescence properties of phosphors prepared via a spray route were analyzed by Wang et al.[20] The results showed that a spherical morphology is good for improving emission intensity.

(16) Lenggoro, I. W.; Okuyama, K. Preparation of Fine Phosphor and Luminescent Micro/Nanoparticles Using Spray Pyrolysis. In *Handbook of Luminescence, Display Materials, and Devices - Inorganic Display Materials*; Nalwa, H. S., Rohwer, L. S., Eds.; American Scientific Publishers: Stevenson Ranch, CA, 2003; Vol. 2, p 327.
(17) Xia, B.; Lenggoro, I. W.; Okuyama, K. *Chem. Mater.* **2002**, *14*, 4969.
(18) Wang, W. N.; Widiyastuti, W.; Lenggoro, I. W.; Kim, T. O.; Okuyama, K. *J. Electrochem. Soc.* **2007**, *154*, J121.
(19) Jung, K. Y.; Lee, C. H.; Kang, Y. C. *Mater. Lett.* **2005**, *59*, 2451.
(20) Wang, L. S.; Zhou, Y. H.; Quan, Z. W.; Lin, J. *Mater. Lett.* **2005**, *59*, 1130.
(21) Shea, L. E.; Mckittrick, J.; Lopez, O. A.; Sluzky, E. *J. Am. Ceram. Soc.* **1996**, *79*, 3257.
(22) Shea, L. E.; McKittrick, J.; Phillips, M. L. F. *J. Electrochem. Soc.* **1998**, *145*, 3165.
(23) Joffin, N.; Dexpert-Ghys, J.; Verelst, M.; Baret, G.; Garcia, A. *J. Lumin.* **2005**, *113*, 249.

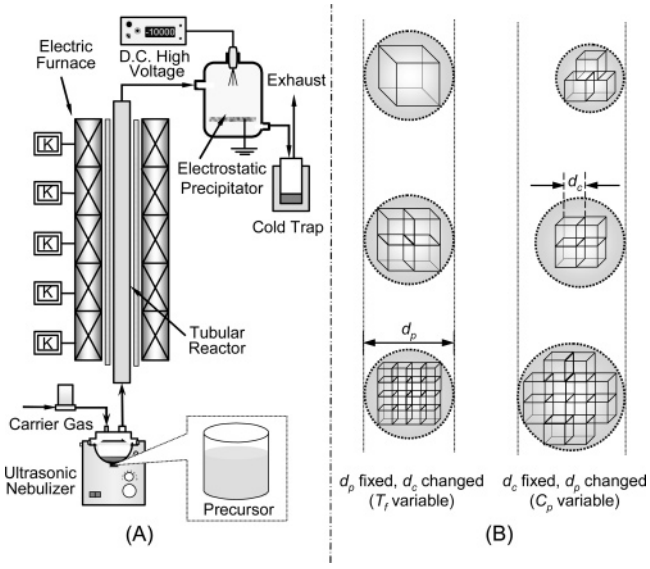

Figure 1. Schematic diagram of experimental setup (A) and procedures (B).

However, few detailed studies focusing on investigations of the effects of particle/crystallite size on the PL properties of submicrometer Y_2O_3:Eu^{3+} powders via the spray route have been reported to date. Further, many previous researchers used additional treatments for improving the PL intensities, especially in industrial applications, such as the use of additives and flux materials in precursors,[13,15,19] which makes it difficult to directly evaluate the effects of particle and crystallite sizes on luminescent intensity.

In this work, we report a systematic experimental study regarding the effects of particle size/crystallinity, as well as chemical composition and surface properties, on the photoluminescent intensity of submicrometer dense phosphor particles with a spherical morphology generated by a spray pyrolysis method. To ensure that a clear explanation could be reached, crystallite size and particle size were controlled independently.

2. Experimental Section

Aqueous solutions of yttrium nitrate ($Y(NO_3)_3 \cdot 6H_2O$, purity > 99.99%) and europium nitrate ($Eu(NO_3)_3 \cdot 6H_2O$, purity > 99.99%) were used as precursors for the preparation of Y_2O_3:Eu^{3+} particles. $Eu(NO_3)_3 \cdot 6H_2O$ was added to a doping level of 6 mol % of europium atoms relative to that of yttrium atoms which gave the optimum doping concentration.[13] All chemicals were purchased from the Kanto Chemical Co., Inc., Tokyo, Japan, and were used without further purification.

The solutions were then atomized by means of an ultrasonic nebulizer operated at 1.7 MHz (NE-U17, Omron Healthcare Co., Ltd., Tokyo, Japan), and the mist was carried by air at 2 L/min into a tubular alumina reactor (1 m in length and 13 mm in inner diameter) maintained at predetermined temperatures, followed by heating for several seconds. The generated mist/droplets were measured by a laser diffraction technique (Spraytec, Malvern Instruments, Ltd., Malvern, Worcestershire, U.K.). The aerosol products were collected in an electrostatic precipitator that was monitored at a temperature of around 150 °C to avoid water condensation. The CSP setup is schematically shown in Figure 1A and has been described in detail in our previous papers.[13,24]

The morphology and grain size of the resulting powders were examined using field-emission scanning electronic microscopy (FE-

SEM, S-5000, Hitachi Corp., Tokyo, Japan) at 20 kV. The inner structure and primary crystallite morphology of the phosphor particles were analyzed by field-emission transmission electronic microscopy (FE-TEM, JEM-3000F, JEOL, Tokyo, Japan) operated at 300 kV. During the TEM analysis, a small amount of Y_2O_3:Eu^{3+} powder was dissolved in acetone and was then subjected to ultrasonication to achieve a well-dispersed suspension. Three drops of the suspension were placed on copper micrometer grids, which were coated with an ultrahigh resolution carbon support film for high magnifying observation (STEM100Cu, Okenshoji Co., Ltd., Tokyo, Japan), after drying the solution naturally. The crystallinity of the crystallites/particles was determined using selected area electron diffraction (SAED) coupled with TEM. Elemental mapping and the chemical composition of the particles were carried out using scanning transmission electron microscopy (STEM) equipped with energy dispersive X-ray spectroscopy (EDS). Crystalline phases were also characterized by an X-ray diffraction (XRD, RINT 2200V, Rigaku Denki, Tokyo, Japan) using nickel-filtered Cu Kα radiation ($\lambda = 1.54$ Å) at 40 kV and 30 mA with a scan step of 0.02° in 2θ and a scan speed of 4°/min. The divergence slit (DS), scatter slit (SS), and receiving slit (RS) are 1°, 1°, and 0.15 mm, respectively. Crystallite size was calculated using the Scherrer equation. The calculation is based on the measurement of full-width at half-maximum (fwhm) values in the corresponding XRD pattern. PL spectra of the phosphors were recorded at room temperature by means of a spectrofluorophotometer (RF-5300PC, Shimadzu Corp., Kyoto, Japan) equipped with a xenon laser source excited at 254 nm. The phosphors were inserted into a cylindrical aluminum holder with a diameter of 4.5 mm and a height of 1.5 mm. The quantum efficiency (QE) of the as-prepared particles was also analyzed using a PL quantum efficiency measurement system (C9920-02, Hamamatsu Photonics, Shizuoka, Japan) under excitation at 254 nm by a 150 W Xe lamp. The CIE1931 (Commission Internationale de l'Eclairage) XY chromaticity coordinate graph (*XY* diagram) was also plotted for further analysis of the phosphors. The chemical properties of the resulting powder surface were analyzed using a Fourier transform infrared (FT-IR) spectrophotometer (IRPrestige-21, Shimadzu Corporation, Kyoto, Japan). The FT-IR measurements were carried out at room temperature with a resolution of 2 cm^{-1} using the conventional KBr pellet technique.

3. Results and Discussion

To investigate the effect of crystallite size, precursors with the same concentration (C_p), namely 0.10 M, were atomized to prepare phosphor particles at various synthesis temperatures (T_f), ranging from 800 °C to 1500 °C. As a result, the sizes of the as-prepared phosphors were consistently around 530 nm. On the other hand, in examining the effect of particle size, precursors at different concentrations, that is, 0.005−0.25 M, were sprayed at a constant synthesis temperature (1000 °C in these cases). Accordingly, the sizes of the resulting powders were in the range from 180 to 850 nm, following the ODOP principle. To eliminate the influence of crystallite size in these cases, a postannealing was applied to the as-prepared sprayed phosphors to maintain a constant crystallite size. This approach for the independent control of crystallite and particle sizes in the spray route is schematically illustrated in Figure 1B.

3.1. Morphology, Particle Size, and Crystallinity Measurements. FE-SEM images of the resulting Y_2O_3:Eu^{3+} submicrometer particles are shown in Figures 2 and S1 (Supporting Information). It can be seen from these images that all samples obtained via the spray route were nonagglomerated spherical particles with smooth surfaces, which is considered to be of benefit in enhancing PL properties. As discussed above, in the case of spraying precursors with the same concentration at various synthesis temperatures, the product particle sizes remain nearly constant (see Figure 2). For example, the particle sizes are 538, 534, and 524 nm at 900 °C, 1300 °C, and 1500 °C, respectively. The slight decrease in particle size with increasing synthesis temperature is due to a sintering effect, which was also observed in the preparation of Pr^{3+}, Al^{3+}-doped strontium titanate ($SrTiO_3$:Pr,Al) and cerium-doped yttrium−gadolinium aluminum garnet ($(Y,Gd)_3Al_5O_{12}$:Ce^{3+}) via the spray route.[25]

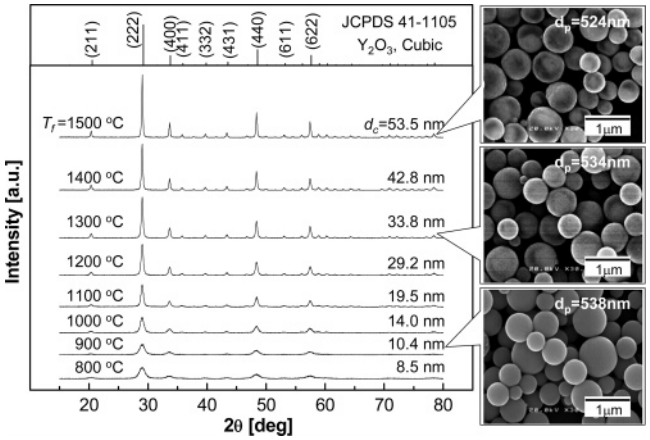

Figure 2. XRD patterns (left) and FE-SEM images (right) of as-prepared Y_2O_3:Eu^{3+} particles from 0.10 M precursor at various synthesis temperatures.

XRD patterns of the resulting particles are presented in Figures 2 and S1 (Supporting Information) as well. They show that the diffraction peaks of 2θ are observed at 20.5, 29.1, 33.8, 35.9, 40.0, 43.5, 48.6, 53.2, and 57.7. These peaks correspond to the (211), (222), (400), (411), (332), (431), (440), (611), and (622) planes, which can be indexed to the pure body-centered cubic (bcc) Y_2O_3 phase (JCPDS No. 41-1105). No impurity peaks and no transition to monoclinic phases were observed, indicating that the powders prepared by the spray route are pure in both chemistry and crystalline phase. Previous studies also showed that cubic Y_2O_3 phases can be formed at synthesis temperatures as low as 800 °C, when the spray route is used.[19] As shown in Figure 2, the peak intensities increase with increasing synthesis temperatures. Very low peak intensities are observed in the cases of 800 °C, 900 °C, and 1000 °C. No (411), (332), (431), and (611) peaks were clearly found even at 1000 °C, indicating a low degree of crystallinity. However, all peaks are assigned starting from 1100 °C, and the peak intensity increases significantly with increasing temperature. Accordingly, the crystallite size calculated from XRD patterns using the Scherrer equation (Scherrer size) shows the same tendency as that for peak intensity. As seen in Figure 2, the crystallite size was calculated to be from 8.5 nm at 800 °C to 53.5 nm at 1500 °C. The reason for this is that the high-

(24) Wang, W. N.; Lenggoro, I. W.; Terashi, Y.; Wang, Y. C.; Okuyama, K. *J. Mater. Res.* **2005**, *20*, 2873.

(25) Wang, W. N.; Kim, S. G.; Lenggoro, I. W.; Okuyama, K. *J. Am. Ceram. Soc.* **2007**, *90*, 425.

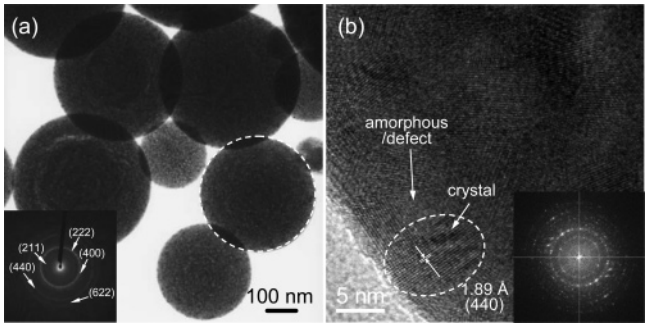

Figure 3. TEM (left) and HR-TEM (right) images of Y_2O_3:Eu^{3+} with the particle size of 538 nm and crystallite size of 10.4 nm; the inset at the left is the SAED pattern, and the right inset is the reduced FFT image. (The dotted circles indicate the perfect spherical and elliptic morphology, respectively.)

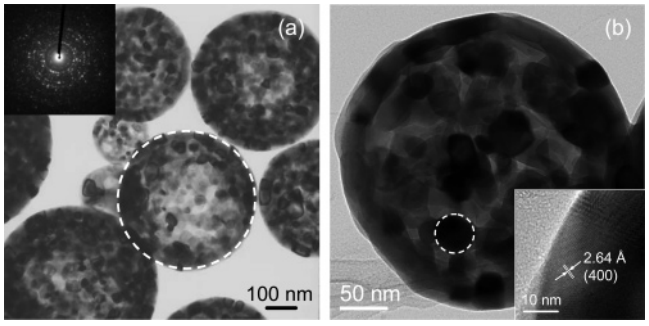

Figure 4. TEM images of Y_2O_3:Eu^{3+} with the particle size of 532 nm and crystallite size of about 42.8 nm; the inset in the left is the SAED pattern and the right insert is the HR-TEM image. (The dotted circles indicate the perfect spherical morphology.)

energy supply from the high synthesis temperature improves nucleation and crystallite growth. Similar results were obtained by Jing et al.[9] and Kang et al.[13] It becomes a general rule that the crystallite size increases with increasing synthesis temperature in the spray route in preparing phosphors such as Zn_2SiO_4:Mn and $LaPO_4$:Ce,Tb.[16]

On the other hand, in the case of various concentrations of precursors sprayed at 1000 °C, the crystallinity did not vary significantly, since the energy supply was constant. The slight difference in crystallite size was caused by differences in energy receiving for precursors at various concentrations. In order to achieve a constant crystallite size, a postannealing was applied to the as-prepared particles. As can be seen from the Figure S1 (Supporting Information), for example, the crystallite sizes of the annealed powders are relatively constant at around 14 nm.

3.2. Crystallite Structure Analyses. To analyze the inner structure of the phosphor particles, TEM was carried out at an accelerating voltage of 300 kV. Two Y_2O_3:Eu^{3+} samples (i.e., Y-16 and Y-23) with similar particle sizes (around 530 nm) and different crystallite sizes, namely, 10.4 and 42.8 nm (as the Scherrer size), respectively, were selected as models. As shown in the left TEM image in Figure 3a, the resulting Y_2O_3:Eu^{3+} produced via the spray route, is all dense/filled particles with a perfect spherical morphology (indicated by a dotted circle) with a mean size of 538 nm. The inset is the SAED pattern recorded from the area, proving the presence of cubic Y_2O_3 phase consistent with the corresponding XRD pattern. However, Debye−Scherrer rings with some diffraction halos are observed in the SAED pattern indicating a low degree of crystallinity. Figure 3b shows a high-resolution transmission electron microscopy (HR-TEM) image of the Y_2O_3:Eu^{3+} crystallites. From the image, single crystallites with an average size of about 10 nm can be seen, which agree well with the calculated Scherrer size. The distance between the adjacent lattice fringes was calculated to be 1.89 Å, which is close to the value for the (440) plane of cubic Y_2O_3. The reduced fast Fourier transform (FFT) image inset in Figure 3b shows a similar phenomenon to that for SAED. However, defects on the crystallite surface and some amorphous phases are observed, suggesting that the crystallinity is low in this case. Further, the single crystallite is slightly deformed, with an elliptic morphology. The low crystallinity and crystallite defects are considered to be the direct reason for the low PL intensity.[21]

Figure 4 shows a sample (Y-23) with a higher crystallinity with nearly the same particle size (i.e., 532 nm). A spherical morphology is observed in this case as well. The particle surface became slightly rough because of the larger primary crystallite sizes. Some vacancies between single crystallites can also be seen in some particles in the left TEM image, which is believed to have little effect on PL intensity. The PL spectra obtained in this case showed a high luminescent peak intensity verifying this assumption, which will be discussed in the next section. Primary crystallites with a nearly spherical morphology of Y_2O_3:Eu^{3+} can clearly be observed in this case. The SAED pattern inserted in the left TEM image in Figure 4 has spotty annular diffraction rings clearly verifying the polycrystalline nature of the samples.[26] The primary crystallite size was determined to be about 40 nm, consistent with the calculated Scherrer size from the corresponding XRD pattern. The HR-TEM image inserted in the right side in Figure 4 shows a perfect crystallite surface in which the distance between adjacent lattice fringes is calculated to be 2.64 Å indicating the (400) plane of the crystallite. A high degree of crystallinity and a larger crystallite size are considered to be the reason for the improved PL intensity which will be discussed below. For comparison, TEM images of Y_2O_3:Eu^{3+} with different particle sizes are shown in Supporting Information (Figure S2).

3.3. PL Characterization. Figure 5 shows PL emission and excitation spectra of Y_2O_3:Eu^{3+} particles with different crystallite sizes at a constant particle size. The emission spectra were recorded under excitation at 254 nm; while the excitation spectra were measured at an emission of 612 nm. From the figure the emission peaks are composed of the characteristic emission lines of Eu^{3+}, corresponding to $^5D_{0,1} \rightarrow {}^7F_J$ ($J = 0, 1, 2, 3, 4, 5, 6$, not in all cases). The main highest emission peak is located at around 612 nm for all samples without a visible shift, caused by $^5D_0 \rightarrow {}^7F_2$, which is a hypersensitive forced electric dipole transition.[1] It is known that the emission wavelengths of Eu^{3+} are determined primarily by their local environment in host crystallites. In the cubic bixbyite type Y_2O_3 (space group *Ia*3), there are

(26) Dhanaraj, J.; Jagannathan, R.; Kutty, T. R. N.; Lu, C. H. *J. Phys. Chem. B* **2001**, *105*, 11098.

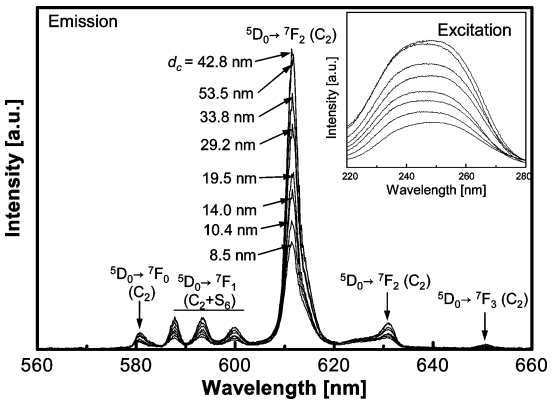

Figure 5. PL emission and excitation (inset) spectra of Y_2O_3:Eu^{3+} powders with different crystallite sizes at a constant particle size.

Table 1. Asymmetric Ratios of $I[^5D_0 \rightarrow {}^7F_2]/I[^5D_0 \rightarrow {}^7F_2]$ of Y_2O_3:Eu^{3+} Particles with Different Crystallite Sizes at a Constant Particle Size

sample	d_p [nm]	d_c [nm]	asymmetric ratio[a] $I[^5D_0 \rightarrow {}^7F_2]/I[^5D_0 \rightarrow {}^7F_1]$
Y-17	543	8.5	3.62/0.38 = 9.53
Y-16	538	10.4	4.22/0.44 = 9.59
Y-15	535	14.0	5.28/0.52 = 10.15
Y-14	537	19.5	5.84/0.57 = 10.24
Y-25	528	29.2	7.48/0.75 = 10.25
Y-24	534	33.8	8.52/0.82 = 10.39
Y-23	532	42.8	9.94/0.94 = 10.57
Y-22	524	53.5	9.82/0.94 = 10.45

[a] $I[^5D_0 \rightarrow {}^7F_2]$ was calculated from PL intensities at 612 nm, while $I[^5D_0 \rightarrow {}^7F_1]$ was calculated from intensities at 593 nm.

two types of cationic sites occupied by Y^{3+} (hence, Eu^{3+}) having either C_2 and S_6 local symmetries (see Supporting Information, Figure S3).[1,26] A total of 75% of these sites are noncentrosymmetric having a C_2 symmetry, and the remaining 25% are centrosymmetric having a S_6 symmetry.[27] The $^5D_0 \rightarrow {}^7F_2$ electric dipole transition occurs at C_2 site, while the $^5D_0 \rightarrow {}^7F_1$ magnetic dipole transition is located at both C_2 and S_6 sites. The intensity ratio of $^5D_0 \rightarrow {}^7F_2$ to $^5D_0 \rightarrow {}^7F_1$, also called the asymmetric ratio,[28] is close to being related to the local environment of Eu^{3+}. Generally, the larger the intensity ratio of $^5D_0 \rightarrow {}^7F_2$ to $^5D_0 \rightarrow {}^7F_1$, the lower the local symmetry.[29] The asymmetric ratios of Y_2O_3:Eu^{3+} particles with various crystallite sizes were also calculated, and the results are shown in Table 1. The results show that the asymmetric ratio increases slightly with increasing crystallite size, which confirms the decrease in local symmetry and hence an increase in red emission ($^5D_0 \rightarrow {}^7F_2$ at 612 nm).

From the excitation spectra inset in Figure 5, the excitation peaks are distributed from 220 to 280 nm, and the maximum peak is located at around 248 nm for all samples, which is assigned to the charge-transfer band (CTB) of Eu^{3+}.[1] The CTB of Y_2O_3:Eu^{3+} corresponds to the electronic transition from the 2p orbital of O^{2-} to the 4f orbital of Eu^{3+} and is closely related to the covalence between O^{2-} and Eu^{3+} and the coordination environment around Eu^{3+}.

(27) Silver, J.; Martinez-Rubio, M. I.; Ireland, T. G.; Fern, G. R.; Withnall, R. *J. Phys. Chem. B* **2001**, *105*, 9107.
(28) Fujihara, S.; Tokumo, K. *Chem. Mater.* **2005**, *17*, 5587.
(29) Yu, L. X.; Song, H. W.; Lu, S. Z.; Liu, Z. X.; Yang, L. M.; Kong, X. G. *J. Phys. Chem. B* **2004**, *108*, 16697.

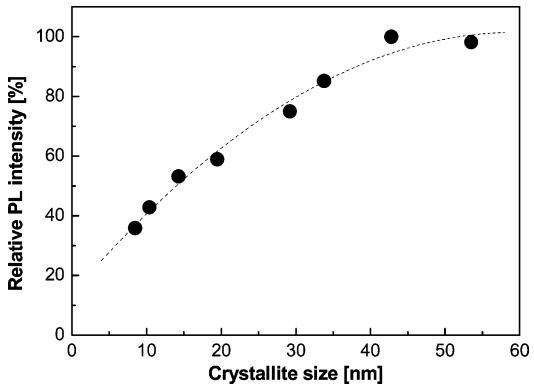

Figure 6. Relationship between the PL intensity and the crystallite size for Y_2O_3:Eu^{3+} powders with a constant particle size.

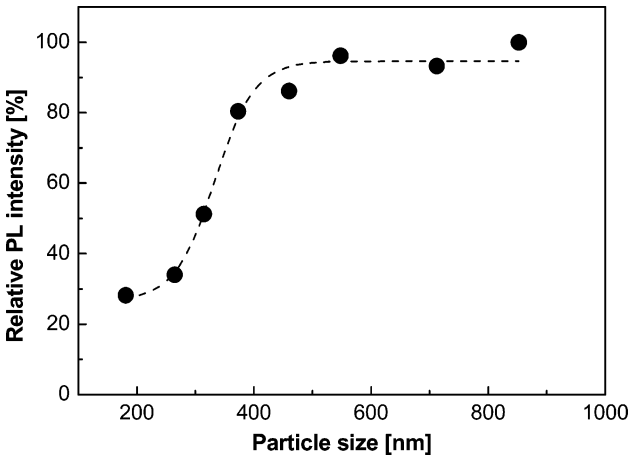

Figure 7. Relationship between PL intensity and particle size for Y_2O_3:Eu^{3+} powders with a constant crystallite size.

The effect of crystallite size on PL intensity is clearly indicated in the figure. The PL intensities at 612 nm in emission spectra gradually increase with increasing crystallite size, as shown in Figures 5 and 6, indicating the strong effect of crystallite size. Fujihara et al. also reported that the luminescent properties of Eu^{3+} are determined by the crystallinity and the lattice symmetry of the host crystal, rather that local distortion induced by substitution.[28] The excitation peak intensity shows a similar tendency as can be seen in the inset in Figure 5. The slight decrease in luminescence intensity after reaching a certain crystallite size is caused by the larger size of the crystallite, which tends to scatter light in particle excitation, leading to a reduction in intensity in luminescence measurements. A similar result was obtained in luminescence measurements by excitation E-beam pulse at low voltage (cathode luminescence).[9]

The effect of particle size on the PL intensity of Y_2O_3:Eu^{3+} was also investigated. The PL emission and excitation spectra of the phosphors were obtained in this case (see Supporting Information, Figure S4), in which the emission and excitation peaks are similar to those presented in Figure 5. The relationship between PL intensity and particle size is plotted in Figure 7. From the figure, a significant increase in PL intensity was observed when the particle diameter was increased from 200 to 500 nm. However, the PL intensity tends to be saturated when the particle size reaches 500 nm. For a particle size of more than 500 nm, the PL intensity is relatively constant. The scattering of incident light inside

Table 2. Particle/Crystallite Parameters and QE of Various Y_2O_3:Eu^{3+} Particles

				CIE coordinates	
sample	d_p [nm]	d_c [nm]	QE [%]	*x*	*y*
Y-9	265	13.3	6.0	0.458	0.289
Y-16	538	10.4	18.31	0.574	0.320
Y-15	535	14.0	22.84	0.590	0.326
Y-11	852	14.8	26.87	0.609	0.331
Y-14	537	19.5	29.43	0.623	0.334
Y-25	528	29.2	37.84	0.624	0.334
Y-23	532	42.8	51.76	0.625	0.338

particles larger than 500 nm tends to increase. Hence, the PL intensity tends to be constant and decrease under some conditions.

To clarify the importance of the effects of crystallite and particle size on the PL intensity of Y_2O_3:Eu^{3+} submicrometer particles, QE measurements were employed as well. The QE of a luminescent material is defined as the ratio of the number of photons emitted to the number of photons absorbed. This ratio is also termed the quantum yield (QY). QE has long been used as a criterion for the selection of luminescent materials for applications in fluorescent lighting, flat panel displays, and more recently, solid-state lighting.[30] Schmechel's group investigated the QE of Y_2O_3:Eu^{3+} nanocrystals prepared in a tubular reactor by chemical vapor synthesis and obtained a QE of only 3−5% following excitation at 253 nm. The low QE was presumed to be due to an increase in the nonradiative excitation rate, caused by structural imperfections in the lattice.[31] Table 2 lists the QE of Y_2O_3:Eu^{3+} phosphors with various particle and crystallite sizes. In the case of particles with a size of 528 nm and a crystallite size of 29.2 nm, the measured QE has been reported to be as high as 37.84%. The QE tends to increase with increasing crystallite size for phosphors with a similar particle size (i.e., around 530 nm). For example, QEs are measured as 18.31%, 22.84%, 29.43%, 37.84%, and 51.76% for Y-16 (d_c = 10.4 nm), Y-15 (d_c = 12.0 nm), Y-14 (d_c = 19.5 nm), Y-25 (d_c = 29.2 nm), and Y-23 (d_c = 42.8 nm), respectively. A similar tendency is also observed for phosphors with different particle sizes but a constant **crystallite** size; that is, the QE increases with increasing particle size. However, it is interesting to note that only a 26.87% QE was obtained in the case of particles with a size larger than 852 nm with relatively low crystallinity (14.8 nm). These results reveal that the crystallite effect plays a more important role in PL intensity than other parameters.

A CIE1931 XY chromaticity coordinate graph (XYdiagram) was also plotted for the further analysis of the phosphors (Figure 8). The CIE1931 graph comprises triangle of R (red), G (green), and B (blue). The purity of red increases with increasing *x* coordinates. The position of a color in the diagram is called the chromaticity point of the color.[32] From the figure, the effects of crystallite and particle sizes on chromaticity can clearly be seen. In the case of a

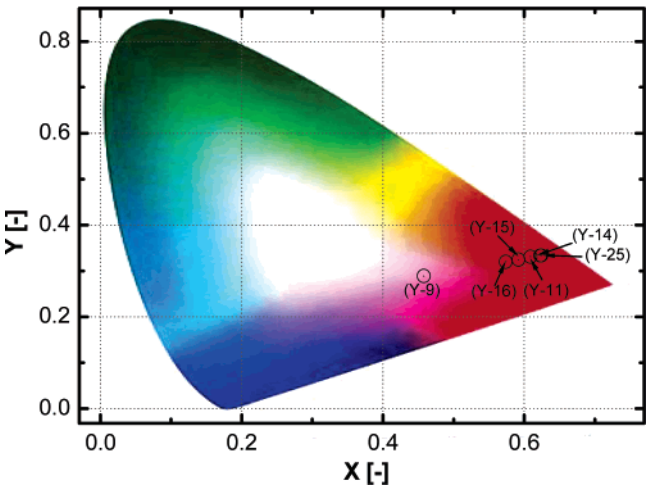

Figure 8. CIE diagram of Y_2O_3:Eu^{3+} powders with different particle and crystallite sizes.

low crystallinity and small size (Y-9), the *x* and *y* chromaticity coordinates are 0.458 and 0.289, respectively. The corresponding color actually can be classified as pink instead of red compared with the standard CIE chromaticity diagram.[32] CIE coordinates of phosphors with increased crystallinity were measured as (0.574, 0.320), (0.590, 0.326), (0.609, 0.331), (0.623, 0.334), (0.624, 0.334), and (0.625, 0.338), for Y-16, Y-15, Y-11, Y-14, Y-25, and Y-23, respectively, indicating an increase in red color purity. The CIE coordinates of Y-25 and Y-23 are close to that of the standard red phosphor.[33] Two main factors are considered as the reason for the phenomena: (1) the asymmetric ratio increases with increasing crystallinity, which has been explained above, and (2) the Eu doping effect becomes stronger in the case of particles with higher crystallinity, resulting in an improved activation degree of Eu^{3+} (hence the improved red color emission).

3.4. Elemental Mapping. As discussed above, chemical composition is also of importance in the luminescent properties of phosphors. To verify the chemical composition inside the phosphor particles, elemental mapping was conducted using STEM with EDS, which is an effective tool for the analysis of elemental distribution.[34,35]Two samples, that is, Y-16 and Y-23, were selected for the measurement. The morphology of the two samples is displayed in the STEM images, Figure 9 a(T1),b(T2), which are the same as those obtained from TEM images in Figures 3 and 4, respectively. The corresponding maps for oxygen (O), yttrium (Y), and europium (Eu) acquired with the use of the X-ray signal emitted from the samples as a probe was scanned across the samples, and the results are shown in Figure 9a,b. From Figure 9 it can be seen that, in the case of particles with a low crystallinity, Y, Eu, and O atoms are

(30) Rohwer, L. S.; Martin, J. E. *J. Lumin.* **2005**, *115*, 77.
(31) Schmechel, R.; Winkler, H.; Li, X. M.; Kennedy, M.; Kolbe, M.; Benker, A.; Winterer, M.; Fischer, R. A.; Hahn, H.; von Seggern, H. *Scr. Mater.* **2001**, *44*, 1213.
(32) Narisada, K.; Kanaya, S. Color vision. In *Phosphor Handbook*; Shionoya, S., Yen, W. M., Eds.; CRC press: New York, 1999; pp 805−809.
(33) Chakhovskoi, A. G.; Hunt, C.; Malinowski, M.; Felter, T.; Talin, A. *J. Vac. Sci. Technol. B* **1997**, *15*, 507.
(34) Feng, X. D.; Sayle, D. C.; Wang, Z. L.; Paras, M. S.; Santora, B.; Sutorik, A. C.; Sayle, T. X. T.; Yang, Y.; Ding, Y.; Wang, X. D.; Her, Y. S. *Science* **2006**, *312*, 1504.
(35) Wang, Z. L.; Zhang, Z.; Liu, Y. Transmission Electron Microscopy and Spectroscopy. In *Handbook of Nanophase and Nanostructured Materials - Characterization*; Wang, Z. L., Liu, Y., Zhang, Z., Eds.; Tsinghua University Press & Kluwer Academic Plenum Publishers: Beijing, China, 2002; Vol. 2, p 93.

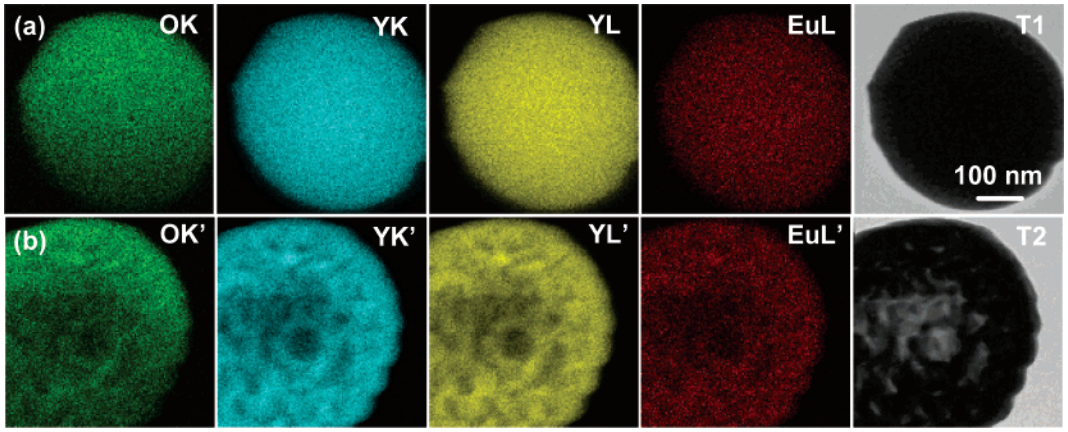

Figure 9. STEM images and elemental mapping of Y_2O_3:Eu^{3+} powders with a constant particle size (around 530 nm) and different crystallite sizes, (a) 10.4 nm (Y-16) and (b) 42.8 nm (Y-23).

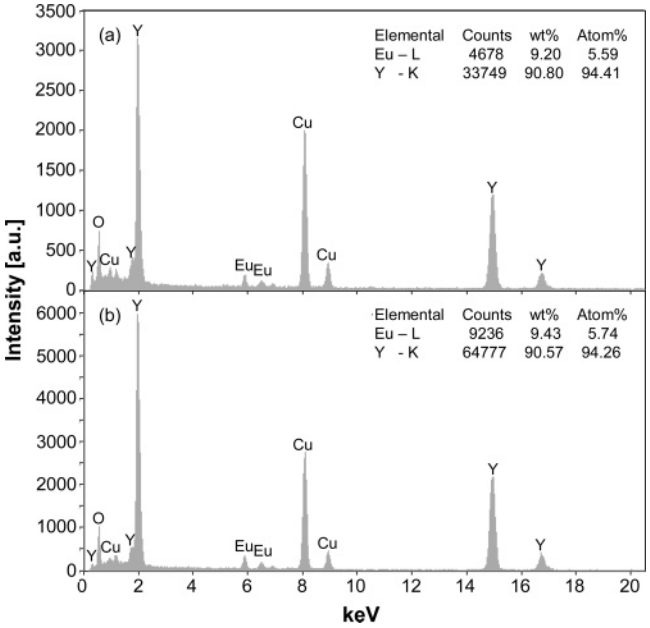

Figure 10. EDS spectra acquired for two Y_2O_3:Eu^{3+} samples with a constant particle size (around 530 nm) and different crystallite sizes, (a) 10.4 nm (Y-16) and (b) 42.8 nm (Y-23).

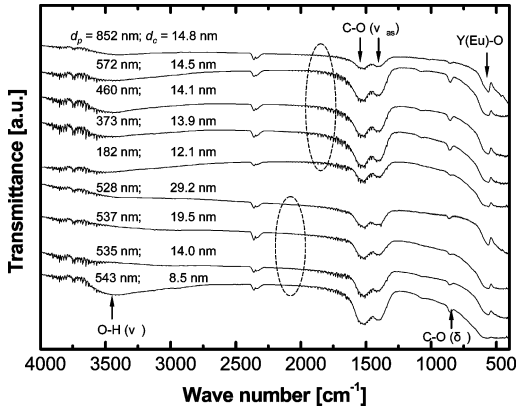

Figure 11. FT-IR spectra of Y_2O_3:Eu^{3+} powders with different particle and crystallite sizes.

well-distributed inside the particle. For reference, corresponding EDS spectra were also recorded from the two samples. From Figure 10, the strongest Y peaks are clearly indicated together with O, Eu, and Cu peaks. It should be noted that the origin of some strong Cu peaks that appeared in the EDS spectra are thought to be from the copper micrometer-grids. No other impurities are evident in the figure implying that the resulting Y_2O_3:Eu^{3+} phosphors are pure in chemical composition. In the case of Y-16, the inset in Figure 10a shows that the relative atomic percentages of Eu and Y are 5.59% and 94.41%, respectively, which agree well with the stoichiometric ratio in the precursor. In the case of particles with a high degree of crystallinity (Y-23), the elemental distribution inside the particle is not well presented because of some vacancies/pores between the single primary crystallites as was found in TEM images as well (Figure 4). However, inside the single crystallites, all of the elements are distributed well, especially on the particle surface. The relative atomic percentages of Eu and Y in this case shown in Figure 10b are 5.74 and 94.26, respectively, which is similar to that in low crystalline particles. The slight increase in Eu in this case is also considered to be one of the reasons for the improved PL intensity. In short, the elements in sprayed phosphor submicrometer particles are well-distributed.

3.5. Surface Chemistry Analyses. FT-IR spectra of the Y_2O_3:Eu^{3+} phosphors with different particle and crystallite sizes were analyzed, to investigate the effect of surface groups on PL intensity. Similar spectra were obtained for all samples as seen in Figure 11. The FT-IR spectra consist mainly of three parts: the first part, with a peak at around 3400 cm^{-1}, due to O−H vibration (ν); the second part, showing peaks at 1518 cm^{-1}, 1405 cm^{-1}, and 842 cm^{-1}, due to C−O asymmetric stretching (ν_{as}) and deformation (δ),[8] due to the absorption of CO_2; and the third part at 558 cm^{-1}, assigned to the absorption of Y_2O_3.[7] A broad OH peak was only found in the case of particles with a low crystallinity, indicating that surface OH groups were not completely removed at low synthesis temperatures (800 °C in this case). From EDS spectra in Figure 10, it is found that only pure Y_2O_3:Eu^{3+} was obtained without detectable carbon contamination. It means that the C−O peaks in FT-IR spectra did not originate from precursors. On the other hand, as is known to all, the particles prepared by the spray route are generally composed of primary nanocrystals. The resulting sprayed particles are actually porous with the pore size in the range of several nanometers. The carbon dioxide absorption on the particle surface or in these pores from air is thus considered as the main reason for C−O peaks in FT-IR spectra. This

may be also one of the reasons for the relatively lower QE compared with that of commercial samples. In the case of particles with different particle size with a constant crystallite size, the Y(Eu)−O peak[7,26] at around 558 cm^{-1} slight increases with increasing particle size, implying that the Eu doping effect is slightly stronger in the case of larger particles. The slightly improved Eu activation efficiency may come from the annealing process. As explained before, to eliminate the crystallite size effect, phosphors prepared from precursors with different concentrations at the same temperature were subjected to annealing for maintenance of the same crystallite size. In the case of higher concentration, the resulting phosphor powders are generally larger in size on the basis of the ODOP principle. However, the primary crystallite size is relatively smaller because the droplet containing precursors with a higher concentration received the same energy as those containing precursors with a lower concentration. To maintain the same crystallite size, larger phosphors need to be annealed at relatively higher temperatures or longer reaction time to receive enough heat energy. In the case of the crystallite size effect, a similar tendency was found as well, that is, the Eu−O doping peak becomes stronger with increasing crystallite size. These findings are considered to be responsible for the improved PL intensities.

4. Conclusions

The effects of crystallite and particle sizes on the PL characteristics of submicrometer phosphor particles (Y_2O_3:Eu^{3+} as a model) were systematically investigated. The crystallite and particle sizes were controlled independently by spraying precursors with the same concentration at various synthesis temperatures and precursors with various concentrations at a constant temperature, respectively. The resulting phosphor particles were analyzed by various methods, such as FE-SEM, TEM, EDS, XRD, SAED, STEM, PL, QE, and FT-IR. The results showed that the phosphor particles produced via the spray route are on the submicrometer sized order with a spherical morphology and are internally dense. Detailed analytical data revealed that the PL intensity increases with increasing crystallite size and particle size, respectively. Crystallite size effect plays a more important role compared with the particle size effect. The optimum crystallite size and particle size are 40 and 500 nm, respectively. It should be noted that the results obtained in this work are mainly for polycrystalline phosphors on submicrometer size order, which can be considered a reference to the future study on nanophosphors and micrometer sized phosphors.

Acknowledgment. We thank Yoko Taguchi and Akihiro Kinoshita for their assistance in spray pyrolysis experiments. Dr. Eishi Tanabe from Hiroshima Prefectural Institute of Industrial Science and Technology is thanked for helping with HR-TEM, EDS analysis, and discussion. The Japan Society for the Promotion of Science (JSPS) and the Ministry of Education, Culture, Sports, Science and Technology (MEXT) of Japan are acknowledged for providing a postdoctoral fellowship (W.-N.W.) and a doctoral scholarship (W.W.), respectively. Grants-in-aid sponsored by MEXT and JSPS are acknowledged (K.O., I.W.L.). This work was also supported in part by NEDO's "Nanotechnology Particle Project" based on funds provided by the Ministry of Economy, Trade, and Industry (METI), Japan.

Supporting Information Available: XRD patterns FE-SEM images of annealed Y_2O_3:Eu^{3+} particles from precursors with various concentrations at 1000 °C, TEM images of two Y_2O_3:Eu^{3+} samples, Y-9 and Y-11, selected area electron diffraction (SAED) patterns, schematic diagram of two crystallographic sites of Y^{3+} in Y_2O_3:Eu^{3+}, energy level diagram of the $4f^6$ configuration of the Eu^{3+} ion in the cubic Y_2O_3 lattice, and PL emission and excitation spectra of Y_2O_3:Eu^{3+} powders (PDF). This material is available free of charge via the Internet at http://pubs.acs.org.

CM062887P